Structural and Magnetic Studies of Manganese(II) Complexes of the Imidazole-Containing Ligand 5-NO_2-salimH [5-NO_2-salimH_2 = 4-(2-((5-Nitrosalicylidene)amino)ethyl)imidazole] with Varying Nuclearity

Michael J. Baldwin,[†] Jeff W. Kampf,[†] Martin L. Kirk,[‡] and Vincent L. Pecoraro*,[†]

Departments of Chemistry, The University of Michigan, Ann Arbor, Michigan 48109-1055, and The University of New Mexico, Albuquerque, New Mexico 87131

Received June 10, 1994[⊗]

Manganese(II) forms structurally diverse complexes of varying nuclearity with the imidazole-containing Schiff base ligand 5-NO_2-salimH_2 [5-NO_2-salimH_2 = 4-(2-((5-nitrosalicylidene)amino)ethyl)imidazole]. The type of complex formed is determined by the type and stoichiometry of carboxylate added to the reaction mixture. The structures of the complexes Mn(5-NO_2-salimH)$_2$, **1**, and [Mn(5-NO_2-salimH)(μ-HCO_2)(CH_3OH)]$_n$, **2**, have been characterized by X-ray crystallography and are compared to the structure of the linear trinuclear Mn(II) complex Mn_3(5-NO_2-salimH)$_2$(μ-CH_3CO_2)$_4$, **3**, which we reported previously [Baldwin, M. J.; Kampf, J. W.; Pecoraro, V. L. *J. Chem. Soc., Chem. Commun.* **1993**, 1741−1743]. Complex **1** is a mononuclear complex with two meridionally bound ligands. It was crystallized in the orthorhombic space group $P2_12_12_1$, with $Z = 8$, $R = 0.0605$, and $R_w = 0.0590$. The unit cell parameters are $a = 17.170(4)$ Å, $b = 17.811(4)$ Å, $c = 18.305(4)$ Å, and $\alpha = \beta = \gamma = 90.000°$. Complex **2** is a polymeric chain with equatorial-to-axial formate bridges in the anti−anti configuration, a meridionally bound 5-NO_2-salimH in the other equatorial positions, and a methanol ligating in the other axial position. It was crystallized in the orthorhombic space group *Pcab* (the alternative setting to *Pbca*), with $Z = 8$, $R = 0.0404$, and $R_w = 0.0433$. The unit cell parameters are $a = 8.070(2)$ Å, $b = 11.895(3)$ Å, $c = 34.29(1)$ Å and $\alpha = \beta = \gamma = 90.000°$. Complex **3** is a linear trimer with 5-NO_2-salimH bound meridionally to each terminal Mn and three bridges from each terminal Mn to the central Mn consisting of the phenolate oxygen of the tridentate ligand, a triatomically bridging acetate, and a monatomically bridging acetate producing a unique (μ-phenolato)-(μ-carboxylato-*O*)(μ-carboxylato-*O*,*O*′) bridging set which may be of relevance to the carboxylate shift concept. Comparison of the manganese-imidazole bond lengths in these complexes to those of the few 6-coordinate Mn(II)−imidazole complexes in the literature provides a range of "normal" Mn(II)−imidazole distances for comparison to structurally characterized biological systems and indicates that complexes in which there are multiple bridges to other manganese ions tend to have shorter Mn−N(imidazole) bonds than mononuclear complexes. The variable temperature and variable field magnetic behavior of **2** and **3** were also studied. **2** displays an intrachain exchange interaction $J = -0.25$ cm^{-1}. The magnetic behavior of **3** is well modeled with an exchange interaction of $J = -1.7$ cm^{-1} between each terminal manganese and the central manganese, with no coupling between the two terminal manganese ions. The zero-field splitting parameter for **3** is measured from the 4.8 K EPR spectrum as $|D| = 0.19$ cm^{-1} for the trimeric unit.

Introduction

Manganese plays an essential structural or catalytic role in many proteins.[1,2] The active sites of several hydrolytic enzymes (i.e., glutamine synthetase[3] and arginase[4]) and redox active enzymes (i.e. Mn catalase[5] and Mn ribonucleotide reductase[6,7]) have been shown to include a dinuclear manganese site which is in the Mn^{II}_2 oxidation state for at least part of the catalytic cycle. Several of these have been shown by X-ray crystallography or by electron spin echo envelope modulation (ESEEM) spectroscopy to include imidazole nitrogens from histidine residues coordinated to the manganese. It is therefore of interest to produce model complexes with imidazole ligation to manganese in order to investigate the structural and electronic effects these ligands may have in the protein sites. In addition, crystallography on several manganese[8,9] and iron[10,11] proteins has shown that carboxylate moieties from amino acid residues bind to the metal sites in a variety of terminal or bridging modes. Lippard has suggested that changes in the carboxylate binding mode, the "carboxylate shift" concept,[12] may be very important in the mechanism of reactivity for these proteins. Understanding the structural, electronic, and magnetic effects of different

[†] The University of Michigan.
[‡] The University of New Mexico.
[⊗] Abstract published in *Advance ACS Abstracts,* September 1, 1995.

(1) Pecoraro, V. L.; Gelasco, A.; Baldwin, M. J. In *Mechanistic Bioinorganic Chemistry*; Thorp, H. H., Pecoraro, V. L., Eds.; ACS Books: New York, 1994. American Chemical Society: Washington, DC.
(2) *Manganese Redox Enzymes*; Pecoraro, V. L., Ed.; VCH Publishers: New York, 1992.
(3) Yamashita, M. M.; Almassy, R. J.; Janson, C. A.; Cascio, D.; Eisenberg, D. *J. Biol. Chem.* **1989**, *264*, 17681−17690.
(4) Reczkowski, R. S.; Ash, D. E. *J. Am. Chem. Soc.* **1992**, *114*, 10992−10994.
(5) Penner-Hahn, J. E. In *Manganese Redox Enzymes*; Pecoraro, V. L., Ed.; VCH Publishers: New York, 1992; pp 29−45.
(6) Willing, A.; Follmann, H.; Auling, G. *Eur. J. Biochem.* **1988**, *175*, 167−173.
(7) Willing, A.; Follmann, H.; Auling, G. *Eur. J. Biochem.* **1988**, *170*, 603−611.
(8) Ludwig, M. L.; Metzger, A. L.; Pattridge, K. A.; Stallings, W. C. *J. Mol. Biol.* **1991**, *219*, 335−358.
(9) Hardman, K. D.; Agarwal, R. C.; Freiser, M. J. *J. Mol. Biol.* **1982**, *157*, 69.
(10) Åberg, A.; Ormö, M.; Nordlund, P.; Sjöberg, B.-M. *Biochemistry* **1993**, *32*, 9845−9850.
(11) Nordlund, P.; Sjöberg, B.-M.; Eklund, H. *Nature* **1990**, *345*, 593−598.
(12) Rardin, R. L.; Tolman, W. B.; Lippard, S. J. *New J. Chem.* **1991**, *15*, 417−430.

0020-1669/95/1334-5252$09.00/0

carboxylate bridging modes in manganese complexes will therefore be useful in gaining insight into the structural details of the active site that may influence the chemical mechanisms of catalysis.

We have begun to probe the coordination chemistry of manganese with the imidazole moiety using the series of tridentate ligands X-salimH_2 [X-salimH_2 = 4-(2-(X-salicylideneamino)ethyl)imidazole; X = 5-NO_2, 3,5-dichloro, 5-Cl, H, or 5-OCH_3] in order to develop coordination complexes to model more accurately the structure and function of biological manganese. In addition to imidazole (the functional group of the amino acid histidine), these ligands contain an imino nitrogen, and a phenolate which is unprotonated and thus negatively charged when coordinated to a metal. The phenolate may be modified by addition of electron-donating or -withdrawing groups in order to vary the potential on the metal to which the ligand is bound. The ligand salimH has been previously reported in complexes of iron,[13] copper,[14] and vanadium.[15,16] We have recently commented[17] on how the unique bridging geometry of a carboxylate-bridged species containing Mn(5-NO_2-salimH) provides an extension of the carboxylate shift concept proposed by Lippard.[12]

In this paper, we discuss the structures and magnetic properties of a series of Mn(II) complexes of 5-NO_2-salimH that, due to the electron-withdrawing properties of the nitro group, tends to stabilize a lower oxidation state of the metal relative to other X-substituted derivatives of $salimH^-$. These complexes have varying nuclearities (monomer, trimer, and polymeric chain) and very different bridging modes depending on subtle differences in the conditions of their synthesis, yet each may be selectively prepared in high yield. We report the structures of the monomer, Mn^{II}(5-NO_2-salimH)$_2$, **1**, and the polymeric chain, [Mn^{II}(5-NO_2-salimH)(CH_3OH)(μ-HCO_2)]$_n$, **2**, and provide a more detailed presentation of the linear trinuclear complex, Mn^{II}_3(5-NO_2-salimH)$_2$(μ-CH_3CO_2)$_4$, **3**.[17] We also analyze the magnetic properties of all three complexes and discuss their EPR spectra.

Experimental Section

The following abbreviations are used throughout the text: 5-NO_2-salimH_2 = 4-(2-((5-nitrosalicylidene)amino)ethyl)imidazole; ImH = imidazole; bpy = bipyridyl; biphme = methoxybis(1-methylimidazol-2-yl)phenylmethane); dmf = N,N-dimethylformamide; H_2saladhp = 1,3-dihydroxy-2-methyl-2-(salicylideneamino)propane; EPR = electron paramagnetic resonance; SQUID = superconducting quantum interference device; SCE = saturated calomel electrode; EXAFS = extended X-ray absorption fine structure.

Materials. All reagents and solvents were used as received (Aldrich), with no attempt to eliminate water or oxygen.

Syntheses. 5-NO_2-salimH_2. This ligand and the other X-salimH_2 derivatives were prepared by the Schiff base condensation of histamine with the appropriately substituted salicylaldehyde. To prepare 20 mmol of 5-NO_2-salimH_2, 3.7 g of histamine dihydrochloride and 2.3 g of KOH were dissolved in 150 mL of hot methanol. Then 3.4 g of 2-hydroxy-5-nitrobenzaldehyde was added and the solution was refluxed for 10 min then cooled to room temperature. The solvent was removed by rotary evaporation, and the resulting yellow powder was brought up in 150 mL of 2:1 CH_2Cl_2−methanol. The undissolved potassium chloride was filtered. The solvent was again removed by rotary evaporation, leaving the ligand as a bright yellow powder in >90% yield.

Table 1. Summary of Crystallographic Data for Mn(5-NO_2-salimH)$_2$·0.5 dmf, **1**, and [Mn(5-NO_2-salimH)(HCO_2)(CH_3OH)]$_n$, **2**

	1	**2**
formula	$C_{24}H_{22}N_8O_6Mn$·0.5 dmf	$C_{14}H_{16}N_4O_6Mn$
mol wt	610.04	391.28
cryst syst	orthorhombic	orthorhombic
space group	$P2_12_12_1$ (No. 19)	*Pcab* (alt. No. 61)
a, Å	17.170(4)	8.070(2)
b, Å	17.811(4)	11.895(3)
c, Å	18.305(4)	34.29(1)
α, deg	90.000	90.000
β, deg	90.000	90.000
γ, deg	90.000	90.000
V, Å^3	5598(2)	3291(1)
Z	8	8
cryst dimens, mm	0.20 × 0.22 × 0.34	0.14 × 0.17 × 0.56
abs coeff (μ), cm^{-1}	5.07	8.07
scan width, deg	−0.8 to +0.8	−0.8 to +0.8
2θ, deg	5−50	5−50
no. of unique reflcns	7040	2890
no. of refined reflcns with (F_o) ≥ 2σ(F)	5951	2530
largest residual, e/Å^3	0.49	0.31
temp, °C	−95	25
R	0.0605	0.0404
R_w	0.0590	0.0433

Mn^{II}(5-NO_2-salimH)$_2$ (1). A 1 mmol (0.26 g) sample of 5-NO_2-salimH_2 and 0.5 mmol (0.12 g) $Mn(CH_3CO_2)_2$·$4H_2O$ were each dissolved in separate 100 mL volumes of warm acetonitrile. The two solutions were poured together, stirred with heating for 1 h, and then cooled to room temperature. The resulting orange powder was washed thoroughly with methanol and then ether and allowed to air dry. The yield was 85%. X-ray quality (yellow multifaceted) crystals were obtained by vapor diffusion of ether into a dmf solution of **1**. Anal. Calcd for the bulk powder of **1**, $MnC_{24}H_{22}N_8O_6$ (fw = 573.5): Mn, 9.6; C, 50.27; H, 3.87; N, 19.55. Found: Mn, 10.0; C, 50.27; H, 3.86; N, 19.22.

[Mn^{II}(5-NO_2-salimH)(CH_3OH)(μ-HCO_2)]$_n$ (2). A 2 mmol (0.57 g) sample of $Mn(NO_3)_2$·$6H_2O$ and 4 mmol (0.26 g) of ammonium formate were dissolved in 100 mL of refluxing methanol. Then 2 mmol (0.52 g) of 5-NO_2-salimH_2 was added, and the mixture was stirred while refluxing for 1 h. The resulting orange powder was filtered and washed with methanol and ether. The yield was 70%. X-ray quality (brown blade-like needle) crystals of **2** were obtained by slow evaporation of the filtrate from the above preparation after addition of an equal volume of acetonitrile. Anal. Calcd for the bulk powder of **2**, $MnC_{14}H_{16}N_4O_6$ (fw = 391.3): Mn, 14.0; C, 42.98; H, 4.12; N, 14.38. Found: Mn, 13.8; C, 42.69; H, 4.09; N, 13.97.

Mn^{II}_3(5-NO_2-salimH)$_2$(μ-CH_3CO_2)$_4$ (3) A 3 mmol (0.74 g) sample of $Mn(CH_3CO_2)_2$·$4H_2O$ was dissolved in 100 mL of warm methanol, 5 mmol (0.41 g) of sodium acetate was added, and the solution was stirred until most of the sodium acetate was dissolved. Then 2 mmol (0.52 g) of 5-NO_2-salimH_2 was added, and the solution was refluxed for 20 min. The solution was allowed to stand open to the air for several days, and yellow microcrystals were filtered off in 50% yield. X-ray quality crystals (amber blocks) were obtained by vapor diffusion of acetonitrile into methanol solutions of **3**. Anal. Calcd for microcrystalline **3**, $Mn_3C_{32}H_{34}N_8O_{14}$ (fw = 919.5); Mn, 17.9; C, 41.80; H, 3.73; N, 12.19. Found: Mn, 17.8; C, 41.88; H, 3.48; N. 12.07.

Collection and Reduction of X-ray Data. X-ray quality crystals were obtained as described above and mounted in glass capillaries. A summary of the crystallographic parameters for **1** and **2** are given in Table 1. The structure of **3** was reported previously.[17] Intensity data were obtained at −95 °C for **1** on a Siemens R3 diffractometer and at room temperature for **2** on a Syntex $P2_1$ diffractometer, using Mo Kα radiation (λ = 0.710 73 Å) monochromatized by a graphite crystal whose diffraction vector was parallel to the diffraction vector of the sample. Three standard reflections were measured every 97 reflections,

(13) Davis, J. C.; Kung, W.-J.; Averill, B. A. *Inorg. Chem.* **1986**, *25*, 394−396.
(14) Latour, J.-M.; Tandon, S. S.; Leonard, G. A.; Povey, D. C. *Acta Crystallogr.* **1989**, *C45*, 598−600.
(15) Cornman, C. R.; Kampf, J.; Pecoraro, V. L. *Inorg. Chem.* **1992**, *31*, 1983−1985.
(16) Cornman, C. R.; Kampf, J.; Lah, M. S.; Pecoraro, V. L. *Inorg. Chem.* **1992**, *31*, 2035−2043.
(17) Baldwin, M. J.; Kampf, J. W.; Pecoraro, V. L. *J. Chem. Soc., Chem. Commun.* **1993**, 1741−1743.

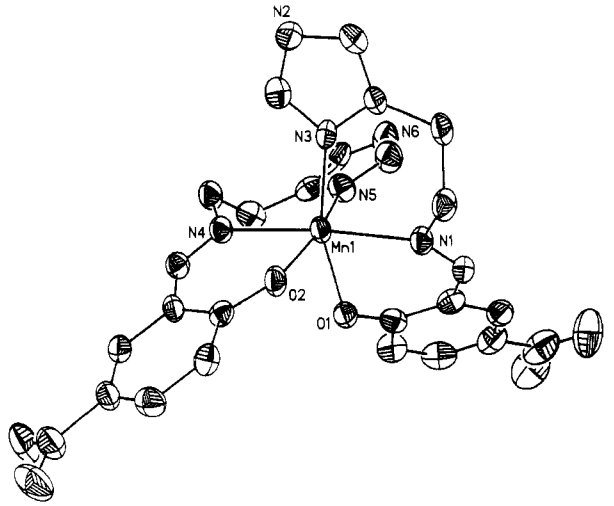

Figure 1. ORTEP plot of one of the two similar molecules in $Mn^{II}(5\text{-}NO_2\text{-salimH})_2 \cdot 0.5$ dmf, **1**.

with random variations of <2%. The data were reduced, the structure was solved, and the model was refined using the SHELXTL PLUS program on a VAX Station 3500. In the subsequent refinement, the function $\sum w(|F_o| - |F_c|)^2$ was minimized where $|F_o|$ and $|F_c|$ are the observed and calculated structure factor amplitudes. The agreement indices $R = \sum(|F_o - F_c|/|F_o|)$ and $R_w = [\sum w(|F_o - F_c|)^2/\sum w(F_o)^2]^{1/2}$ were used to evaluate the results. Atomic scattering factors are taken from The International Tables for X-ray Crystallography. Hydrogen atoms were located but not refined, and placed at a fixed distance of 0.96 Å from the carbon atoms. The hydrogen atoms were given common isotropic temperature factors which were allowed to refine as free variables to values of 0.048(3) Å^2 for **1** and 0.066(3) Å^2 for **2**. Fractional atomic coordinates and isotropic temperature factors of non-hydrogen atoms are given in tables 2 and 3, and selected bond distances and angles are given in tables 4 and 5, for **1** and **2**, respectively.

Additional Methods. Magnetic Susceptibility. Magnetic susceptibility measurements were made on well ground solid samples by a Quantum Design model MPMS superconducting quantum interference device (SQUID). The measurements were calibrated using a recrystallized $HgCo(NCS)_4$ standard.[18] The appropriate diamagnetic corrections were made.

Standard library routines for matrix diagonalization and function minimization were used in the analysis of the data. Susceptibility and magnetization routines incorporating full-matrix diagonalization and spatial averaging were developed by the author at The University of New Mexico.

Electron Paramagnetic Resonance. Electron paramagnetic Resonance (EPR) spectra were obtained using a Bruker ER 200E-SRC controller attached to a Varian Associates magnet. Data were collected at X-band frequencies (9.1 GHz) in a microwave cavity enclosed by an Oxford liquid helium dewar allowing temperature control down to near 4.2 K.

Solution Molecular Weight Measurements. The molecular weight of **2** dissolved in dmf (in order to determine its nuclearity in solution) was determined by vapor pressure osmometry (Galbraith Laboratories, Inc., Knoxville, TN).

Results and Discussion

Variations in the nuclearity and bridging modes of the Mn^{II}-(5-NO_2-salimH) complexes can be acheived by controlling the amount or type of carboxylate used in the reaction mixture. So far, mononuclear (**1**), trinuclear (**3**), and polymeric (**2**) complexes have been structurally characterized. The structures, electrochemistry, and magnetic behavior of these complexes are described below.

$Mn^{II}(5\text{-}NO_2\text{-salimH})_2 \cdot 0.5$ DMF (1). Complex **1** is the dominant product in the reaction of Mn(II) salts with 5-NO_2-

(18) Nelson, D.; ter Haar, L. W. *Inorg. Chem.* **1993**, *32*, 182−188.

Table 2. Fractional Coordinates and Isotropic Thermal Parameters for Non-Hydrogen Atoms in Each Crystallographically Independent Molecule of **1**

atom	*x*	*y*	*z*	*U*(eq)
Mn1	−0.00327(4)	0.04882(4)	0.98119(4)	0.0278(2)
O1	0.0321(2)	−0.0143(2)	1.0765(2)	0.034(1)
O2	−0.0707(2)	0.1254(2)	1.0467(2)	0.032(1)
O3	0.3825(3)	−0.1024(4)	1.1065(4)	0.087(3)
O4	0.3273(4)	−0.2057(3)	1.1434(3)	0.083(2)
O5	−0.3768(3)	0.0371(3)	1.2078(3)	0.060(2)
O6	−0.3602(3)	0.1495(3)	1.2508(3)	0.060(2)
N1	0.1137(3)	0.1055(3)	1.0053(2)	0.033(1)
N2	−0.0452(3)	0.1682(3)	0.7800(3)	0.038(2)
N3	0.0004(3)	0.1183(3)	0.8820(2)	0.032(1)
N4	−0.1241(3)	−0.0071(2)	0.9693(2)	0.032(1)
N5	0.0416(3)	−0.0480(3)	0.9172(3)	0.038(2)
N6	0.1162(3)	−0.1153(3)	0.8457(3)	0.056(2)
N7	0.3256(4)	−0.1403(4)	1.1199(4)	0.068(3)
N8	−0.3421(3)	0.0974(3)	1.2101(3)	0.047(2)
C1	0.1000(4)	−0.0429(3)	1.0841(3)	0.036(2)
C2	0.1095(4)	−0.1171(3)	1.1128(4)	0.043(2)
C3	0.1812(4)	−0.1486(4)	1.1241(4)	0.050(2)
C4	0.2478(4)	−0.1072(4)	1.1086(3)	0.048(2)
C5	0.2427(4)	−0.0350(3)	1.0809(3)	0.041(2)
C6	0.1702(4)	−0.0025(3)	1.0673(3)	0.037(2)
C7	0.1713(3)	0.0729(3)	1.0367(3)	0.034(2)
C8	0.1277(3)	0.1820(3)	0.9765(3)	0.039(2)
C9	0.1296(3)	0.1846(4)	0.8929(3)	0.042(2)
C10	0.0532(3)	0.1718(3)	0.8564(3)	0.035(2)
C11	0.0260(3)	0.2026(4)	0.7939(3)	0.042(2)
C12	−0.0561(3)	0.1199(3)	0.8333(3)	0.035(2)
C13	−0.1368(3)	0.1207(3)	1.0799(3)	0.028(2)
C14	−0.1591(3)	0.1760(3)	1.1327(3)	0.034(2)
C15	−0.2250(3)	0.1693(3)	1.1739(3)	0.037(2)
C16	−0.2737(3)	0.1076(3)	1.1627(3)	0.035(2)
C17	−0.2581(3)	0.0558(3)	1.1093(3)	0.034(2)
C18	−0.1915(3)	0.0616(3)	1.0668(3)	0.030(2)
C19	−0.1819(3)	0.0039(3)	1.0113(3)	0.033(2)
C20	−0.1316(4)	−0.0700(4)	0.9171(3)	0.042(2)
C21	−0.0731(4)	−0.1332(3)	0.9341(4)	0.045(2)
C22	0.0070(4)	−0.1166(3)	0.9055(3)	0.038(2)
C23	0.1077(4)	−0.0509(4)	0.8801(4)	0.049(2)
C24	0.0522(4)	−0.1566(4)	0.8606(4)	0.051(2)
Mn2	0.23690(5)	0.25773(4)	0.26457(4)	0.0274(2)
O7	0.3386(2)	0.3017(2)	0.3196(2)	0.030(1)
O8	0.3032(2)	0.1670(2)	0.2229(2)	0.036(1)
O9	0.3387(3)	0.3656(3)	0.6553(2)	0.062(2)
O10	0.4244(3)	0.4449(3)	0.6190(3)	0.060(2)
O11	0.5695(3)	0.0871(3)	0.0054(4)	0.091(3)
O12	0.5168(3)	0.1801(3)	−0.0534(3)	0.063(2)
N9	0.2158(3)	0.2064(3)	0.3772(3)	0.040(2)
N10	0.0291(3)	0.1647(3)	0.1658(3)	0.047(2)
N11	0.1259(3)	0.2019(3)	0.2352(3)	0.037(1)
N12	0.2569(3)	0.3059(2)	0.1500(2)	0.030(1)
N13	0.0878(3)	0.4405(3)	0.3381(2)	0.036(1)
N14	0.1752(3)	0.3628(3)	0.2925(3)	0.034(1)
N15	0.3768(4)	0.3956(3)	0.6063(3)	0.046(2)
N16	0.5191(3)	0.1372(3)	−0.0006(4)	0.057(2)
C25	0.3448(3)	0.3238(3)	0.3873(3)	0.029(2)
C26	0.4003(4)	0.3793(3)	0.4055(3)	0.039(2)
C27	0.4111(4)	0.4026(3)	0.4760(3)	0.042(2)
C28	0.3656(4)	0.3715(3)	0.5312(3)	0.038(2)
C29	0.3122(3)	0.3169(3)	0.5158(3)	0.034(2)
C30	0.2994(3)	0.2925(3)	0.4448(3)	0.032(2)
C31	0.2441(3)	0.2326(3)	0.4365(3)	0.038(2)
C32	0.1609(5)	0.1430(4)	0.3854(4)	0.060(3)
C33	0.0804(5)	0.1631(5)	0.3617(4)	0.077(3)
C34	0.0704(4)	0.1705(4)	0.2800(4)	0.060(3)
C35	0.0101(5)	0.1480(5)	0.2368(4)	0.075(3)
C36	0.0969(4)	0.1989(4)	0.1701(3)	0.041(2)
C37	0.3508(3)	0.1598(3)	0.1681(3)	0.032(2)
C38	0.4019(4)	0.0982(3)	0.1651(4)	0.046(2)
C39	0.4571(4)	0.0905(4)	0.1108(4)	0.049(2)
C40	0.4610(3)	0.1438(3)	0.0560(4)	0.041(2)
C41	0.4104(3)	0.2054(3)	0.0554(3)	0.037(2)
C42	0.3551(3)	0.2140(3)	0.1104(3)	0.029(2)
C43	0.3065(3)	0.2806(3)	0.1037(3)	0.031(2)
C44	0.2151(3)	0.3746(4)	0.1285(3)	0.040(2)
C45	0.2243(4)	0.4374(3)	0.1851(4)	0.045(2)
C46	0.1737(3)	0.4274(3)	0.2510(3)	0.031(2)
C47	0.1201(3)	0.4750(3)	0.2792(3)	0.037(2)
C48	0.1226(3)	0.3734(4)	0.3443(3)	0.039(2)

Table 3. Selected Bond Lengths (Å) and Bond Angles (deg) for the Two Crystallographically Independent Molecules in the Asymmetric unit of **1**

Mn1−O1	2.162(4)	Mn2−O7	2.162(4)
Mn1−O2	2.154(4)	Mn2−O8	2.119(4)
Mn1−N1	2.291(4)	Mn2−N9	2.284(5)
Mn1−N3	2.199(4)	Mn2−N11	2.215(5)
Mn1−N4	2.312(4)	Mn2−N12	2.291(4)
Mn1−N5	2.222(5)	Mn2−N14	2.210(5)
N1−Mn1−N3	83.5(2)	N1−Mn1−N4	174.2(2)
N1−Mn1−N5	98.0(2)	N3−Mn1−N4	101.0(2)
O1−Mn1−O2	91.8(1)	N3−Mn1−N5	89.5(2)
O1−Mn1−N1	80.0(1)	O1−Mn1−N3	162.0(2)
O1−Mn1−N4	96.0(1)	N4−Mn1−N5	85.8(2)
O1−Mn1−N5	85.7(2)	O2−Mn1−N1	94.9(1)
O2−Mn1−N3	96.8(2)	O2−Mn1−N4	81.0(1)
O2−Mn1−N5	166.2(2)	O7−Mn2−O8	90.6(1)
O7−Mn2−N9	81.5(2)	O7−Mn2−N11	165.9(2)
O7−Mn2−N12	99.8(1)	O7−Mn2−N14	88.4(2)
O8−Mn2−N9	96.0(2)	O8−Mn2−N11	91.8(2)
O8−Mn2−N12	82.9(2)	O8−Mn2−N14	170.6(2)
N9−Mn2−N11	84.4(2)	N9−Mn2−N12	178.3(2)
N9−Mn2−N14	93.1(2)	N11−Mn2−N12	94.3(2)
N11−Mn2−N14	91.4(2)	N12−Mn2−N14	88.1(2)

salimH_2 and 1 equiv of base per ligand. The base may be a carboxylate provided there is only enough carboxylate present to stoichiometrically accept the proton released upon binding a phenolate of the ligand to the metal. In the presence of excess carboxylate, structures such as **2** or **3** will result. Complex **1** is insoluble in methanol and precipitates upon its formation, but it is quite soluble in dmf. The cyclic voltammogram of **1** in dmf shows a pseudoreversible (ΔE = 104 mV, i_a/i_c = 0.7) Mn(II/III) couple at +290 mV vs SCE.

The crystallographically determined structure of **1** is shown in Figure 1 with the fractional coordinates and isotropic thermal parameters for non-hydrogen atoms provided in Table 2. One of the two similar but crystallographically inequivalent molecules in the noncentrosymmetric $P2_12_12_1$ unit cell is shown. Both molecules in the unit cell consist of the same chiral isomer, Δ or C (clockwise) as described by Hahn et al. for ML_2 complexes with meridional tridentate ligands,[19] differing only slightly in their bond lengths. The bond distances and angles for the manganese coordination sphere of each molecule are given in Table 3. The tridentate ligands are meridionally bound, so that the imine nitrogens are necessarily trans to each other and each phenolate oxygen is trans to the imidazole nitrogen of the same ligand. This meridional coordination is likely imposed by the C−N double bond at the imine nitrogen, and is common to the structures reported for salimH with other metals.[13-16] The distances between the metal and the ligating atoms are typical of Mn(II) complexes. The average Mn−N(imidazole) distance is 2.21 Å [*vide infra*]. In **1**, as well as in **2** and **3**, the "N2" nitrogen of the imidazole is always bound to the Mn and the "N4" nitrogen is monoprotonated. The average Mn−N(imine) distance is 2.29 Å, and the average Mn-O(phenolate) distance is 2.15 Å. Complex **1** is structurally similar to the Fe(III) complex FeL_2^+, where L is the unsubstituted ligand, salimH, except that the Fe complex was crystallographically characterized as the opposite (Λ or A (anticlockwise)) chiral isomer.[13]

$[Mn^{II}(5\text{-}NO_2\text{-}salimH)(CH_3OH)(\mu\text{-}HCO_2)]_n$ (2). In methanol solutions of Mn(II), 5-NO_2-salimH, and more formate than is required for ligand deprotonation, the dominant product is the linear polymer, $[Mn^{II}(5\text{-}NO_2\text{-}salimH)(CH_3OH)(\mu\text{-}HCO_2)]_n$, **2**. Figure 2 shows four manganese links of the polymeric chain,

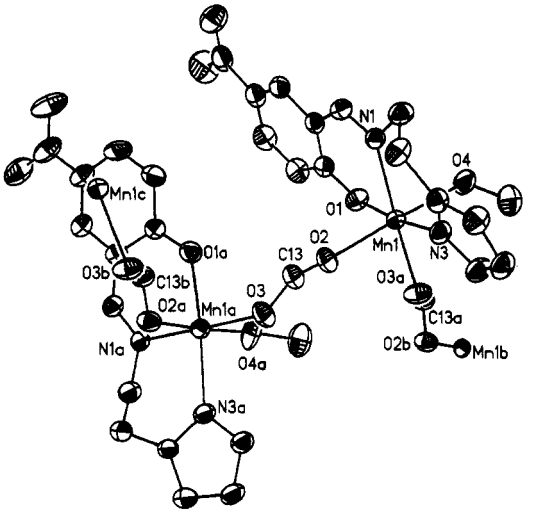

Figure 2. ORTEP plot of four manganese links of the polymeric chain, $[Mn^{II}(5\text{-}NO_2\text{-}salimH)(\mu\text{-}HCO_2)(CH_3OH)]_n$, **2**, two of which are shown with their complete ligand sets.

Table 4. Fractional Coordinates and Isotropic Thermal Parameters for Non-Hydrogen Atoms in **2**

atom	*x*	*y*	*z*	*U*(eq)
Mn1	0.12503(5)	0.93561(3)	0.65009(1)	0.0309(1)
O1	0.0992(3)	0.8515(2)	0.59716(5)	0.0440(7)
O2	−0.1042(2)	0.8593(2)	0.67238(5)	0.0406(6)
O3	−0.2450(3)	0.7005(2)	0.67737(5)	0.0467(7)
O4	0.3699(3)	1.0046(2)	0.62614(7)	0.0667(9)
O5	−0.3649(4)	1.0004(3)	0.46190(7)	0.082(1)
O6	−0.3024(4)	0.8327(3)	0.44369(7)	0.093(1)
N1	0.0010(3)	1.0776(2)	0.61933(6)	0.0351(7)
N2	0.2238(3)	1.1116(2)	0.75776(7)	0.0496(9)
N3	0.1431(3)	1.0413(2)	0.70180(6)	0.0403(8)
N4	−0.2947(4)	0.9110(3)	0.46731(8)	0.061(1)
C1	0.0043(4)	0.8678(2)	0.56814(7)	0.0362(9)
C2	−0.0171(4)	0.7809(3)	0.53986(9)	0.052(1)
C3	−0.1135(4)	0.7942(3)	0.50779(9)	0.053(1)
C4	−0.1952(4)	0.8956(3)	0.50167(8)	0.047(1)
C5	−0.1803(4)	0.9821(3)	0.52799(8)	0.043(1)
C6	−0.0830(3)	0.9714(2)	0.56144(7)	0.0358(9)
C7	−0.0724(4)	1.0694(2)	0.58598(8)	0.0390(9)
C8	−0.0010(4)	1.1896(2)	0.63750(8)	0.047(1)
C9	−0.0642(4)	1.1846(3)	0.67956(8)	0.049(1)
C10	0.0575(4)	1.1402(2)	0.70839(8)	0.0381(9)
C11	0.1074(4)	1.1840(3)	0.74297(8)	0.048(1)
C12	0.2419(4)	1.0280(3)	0.73226(8)	0.047(1)
C13	−0.1577(4)	0.7678(3)	0.65937(8)	0.041(1)
C14	0.5342(4)	0.9897(4)	0.6358(1)	0.079(2)

Table 5. Selected Bond Lengths (Å) and Bond Angles (deg) for **2**

Mn1−O1	2.083(2)	Mn1−N1	2.229(2)
Mn1−O2	2.198(2)	Mn1−N3	2.178(2)
Mn1−O3a	2.144(2)	Mn1a−O3	2.144(2)
Mn1−O4	2.292(2)		
N1−Mn1−N3	88.73(8)	O2−Mn1−N1	95.71(8)
O1−Mn1−O2	91.17(7)	O2−Mn1−N3	90.65(8)
O1−Mn1−O3a	93.79(7)	O3a−Mn1−O4	90.28(8)
O1−Mn1−O4	86.90(8)	O3a−Mn1−N1	176.87(8)
O1−Mn1−N1	84.66(8)	O3a−Mn1−N3	92.76(8)
O1−Mn1−N3	173.28(8)	O4−Mn1−N1	86.93(9)
O2−Mn1−O3a	87.03(7)	O4−Mn1−N3	91.58(9)
O2−Mn1−O4	176.59(8)		

with two of them showing the entire ligand set. The fractional coordinates and isotropic thermal parameters for non-hydrogen atoms in **2** are provided in Table 4, and the bond distances and angles of the manganese coordination sphere are listed in Table 5. All interchain Mn−Mn distances are greater than 10 Å with no hydrogen bonding between chains. This polymer consists of chains of Mn(II) ions with a single formate bridge connecting

(19) Hahn, F. E.; McMurry, T. J.; Hugi, A.; Raymond, K. N. *J. Am. Chem. Soc.* **1990**, *112*, 1854−1860.

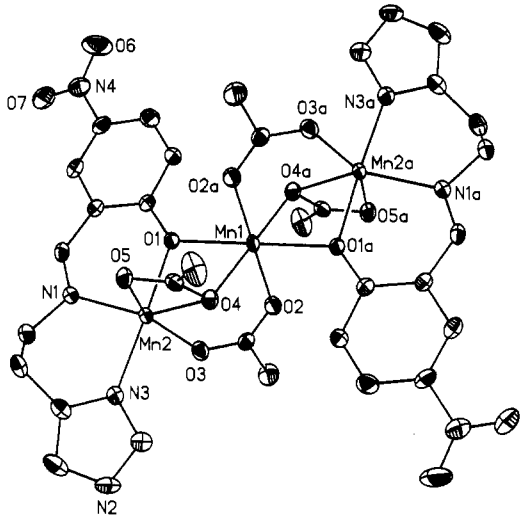

Figure 3. ORTEP plot of $Mn^{II}_3(5\text{-}NO_2\text{-}salimH)_2(\mu\text{-}CH_3CO_2)_4$, **3**. (The structure of this complex was previously reported in ref 17. Reprinted with permission. Copyright 1993 Royal Society of Chemistry.)

each manganese to the next with a Mn−Mn separation of 5.98 Å. The formates bridge in an anti−anti configuration, and are coordinated in equatorial and axial positions of the manganese (Mn(1)−O(3A) = 2.14 Å, Mn(1)−O(2) = 2.20 Å), where the equatorial plane includes the three ligating atoms of 5-NO_2-salimH and a formate oxygen. This leads to an equatorial to axial connectivity that results in a staggered chain, with the equatorial planes of the manganese canted by 62.8° with respect to the Mn(1)−Mn(1c) vector. A straight line extends through every other manganese in the chain. The methanol (Mn(1)−O(4) = 2.29 Å) is in the other axial position, trans to a formate bridge. The equatorially bound formate bridge is trans to the imine nitrogen of 5-NO_2-salimH. The distances between the manganese and the coordinated 5-NO_2-salimH atoms [Mn(1)−O(1)(phenolate) = 2.08 Å; Mn(1)−N(1)(imine) = 2.23 Å; Mn(1)−N(3)(imidazole) = 2.18 Å] in **2** are all shorter than those in **1**, since the methanol and the bridging formates are weaker donors than those in the second 5-NO_2-salimH of **1**.

Mn^{II}_3(5-NO_2-salimH)$_2$(μ-CH_3CO_2)$_4$ (3). Addition of excess acetate to a solution of Mn(II) and 5-NO_2-salimH results in the linear trimer, **3**. While this complex can be easily recrystallized in high yield from methanol, it dissociates in solution to Mn(II) monomers (*vide infra*). Addition of an equimolar amount of formate, relative to acetate, to this solution results in formation of **2** in high yield relative to the limiting reagent, 5-NO_2-salimH. This indicates that formation of **2** is preferred over that of **3**, regardless of the Mn:ligand stoichiometry.

We have previously reported the structure of **3**,[17] shown in Figure 3. The central Mn(1) sits on an inversion center, and the Mn(1)−Mn(2) distance is 3.27 Å. As in **1** and **2**, the 5-NO_2-salimH is bound meridionally to each terminal Mn; however in **3**, the phenolate oxygen bridges monatomically to the central Mn. This results in a shortened Mn−N(imidazole) distance (2.16 Å) in **3** relative to either **1** or **2**, while the Mn−N(imine) distance (2.23 Å) in **3** is very close to that in **2**. In addition to the phenolate bridge, there are two acetate bridges between each terminal Mn and the central Mn, one bridging in the normal triatomic (μ-acetato-*O*,*O*′) syn-syn configuration, and the other in a monatomic (μ-acetato-*O*) mode, with the nonbridging oxygen bound in the remaining coordination position of the terminal Mn. The bond distances and angles between the Mn ions and the coordinated atoms are listed in Table 6.

While there are several Mn and Fe complexes with bis(μ-carboxylato-*O*,*O*′), (μ-carboxylato-*O*) bridging sets which have been reported,[12,20−22] **3** represents the only complex of either of these metals containing a (μ-carboxylato-*O*,*O*′), (μ-carboxylato-*O*) bridging set with an additional monatomic bridge (μ-phenolato in this case) such as the oxo or hydroxo bridges present in some dinuclear Mn and Fe protein active sites. We have discussed this novel bridging geometry[17] with respect to the "carboxylate shift" idea developed by Lippard. The Mn−Mn distance in **3** is significantly shorter than for the bis(μ-carboxylato-*O*,*O*′), (μ-carboxylato-*O*) bridged Mn(II) trimers,[12] since the monatomic phenolate bridge results in edge-shared octahedra for the adjacent Mn coordination spheres, while a second triatomic carboxylate bridge in its place results in corner-shared octahedra, and a correspondingly longer Mn−Mn distance.

Table 6. Selected Bond Lengths (Å) and Angles (deg) in $Mn_3(5\text{-}NO_2\text{-}salimH)_2(CH_3CO_2)_4$, **3**[17]

Mn(1)−O(1)	2.261(2)	Mn(2)−O(4)	2.309(2)
Mn(1)−O(2)	2.100(2)	Mn(2)−O(5)	2.371(2)
Mn(1)−O(4)	2.264(2)	Mn(2)−N(1)	2.232(2)
Mn(2)−O(1)	2.124(2)	Mn(2)−N(3)	2.159(2)
Mn(2)−O(3)	2.102(2)		
Mn1−O1−Mn2	96.38(7)	Mn1−O4−Mn2	91.28(7)
O1a−Mn1−O4	100.32(7)	O2−Mn1−O2a	180.0(7)
O2−Mn1−O4	92.71(7)	O2−Mn1−O4a	87.29(7)
O1−Mn1−O1a	180.000	O1−Mn1−O2	92.74(7)
O4−Mn1−O4a	180.0(4)	O1−Mn1−O2a	87.26(7)
O1−Mn1−O4	79.68(7)		
O4−Mn2−O5	56.18(7)	O4−Mn2−N1	148.78(8)
O4−Mn2−N3	103.85(8)	O3−Mn2−O4	92.06(8)
O3−Mn2−O5	147.84(8)	O3−Mn2−N1	116.79(9)
O3−Mn2−N3	88.25(8)	O1−Mn2−O3	90.23(8)
O1−Mn2−O4	81.58(7)	O1−Mn2−O5	89.88(7)
O5−Mn2−N1	95.31(8)	O1−Mn2−N1	86.38(8)
O5−Mn2−N3	94.27(8)	O1−Mn2−N3	174.41(9)
N1−Mn2−N3	89.50(9)		

Manganese−Imidazole Distances. Many manganese proteins make use of the imidazole moiety of the histidine amino acid as a ligating group for the metal. It will thus be of use in interpreting the structural data obtained by X-ray crystallography or EXAFS spectroscopy on these manganese-containing proteins, which may have unusual coordination geometries or Mn−ligand bond lengths due to the constraints of the protein structure, to determine a range of "normal" Mn(II)−N(imidazole) bond lengths for comparison. The structures reported here for **1**, **2**, and **3** add several additional examples to the small number of 6-coordinate manganese(II) complexes containing imidazole or methylimidazole ligands. These small molecule complexes do not have the constraints on geometry and bond lengths imposed by the protein environment and may therefore be considered to have Mn−N bond lengths which are determined primarily by the manganese-imidazole interaction rather than other "external" constraints.

Previously reported 6-coordinate manganese(II)−imidazole complexes have Mn−N bonds with a wide variety of lengths, from 2.15 to 2.28 Å. These structures can be divided into two categories, however: mononuclear manganese complexes[23−25] and multinuclear manganese complexes in which three of the

(20) Rardin, R. L.; Poganiuch, P.; Bino, A.; Goldberg, D. P.; Tolman, W. B.; Liu, S.; Lippard, S. J. *J. Am. Chem. Soc.* **1992**, *114*, 5240−5249.
(21) Ménage, S.; Vitols, S. E.; Bergerat, P.; Codjovi, E.; Kahn, O.; Girerd, J.-J.; Guillot, M.; Solans, X.; Calvet, T. *Inorg. Chem.* **1991**, *30*, 2666−2671.
(22) Osawa, M.; Singh, U. P.; Tanaka, M.; Moro-oka, Y.; Kitajima, N. *J. Chem. Soc., Chem. Commun.* **1993**, 310−311.
(23) Garrett, T. P. J.; Guss, J. M.; Freeman, H. C. *Acta Crystallogr.* **1983**, *C39*, 1031−1034.
(24) Garrett, T. P. J.; Guss, J. M.; Freeman, H. C. *Acta Crystallogr.* **1983**, *C39*, 1027−1031.

Table 7. Comparison of Magnetic Parameters

complex	μ_{eff} (300 K), μ_B	$-J$, cm^{-1}	ground state	ref
$Mn^{II}(5\text{-}NO_2\text{-salimH})_2$, **1**	6.01	n.a.	$^5/_2$	this work
$[Mn^{II}(5\text{-}NO_2\text{-salimH})(\mu\text{-}HCO_2)(CH_3\text{-}OH)]_n$, **2**	5.71 (per Mn)	0.25	*a*	this work
$Mn^{II}_3(5\text{-}NO_2\text{-salimH})_2(\mu\text{-}CH_3CO_2)_4$, **3**	10.03	1.7	$^5/_2$	this work
$Mn^{II}_3(bpy)_2(\mu\text{-}CH_3CO_2)_6$	9.75 (285 K)	2.2	$^5/_2$	21
$Mn^{II}_3(BIPhMe)_2(\mu\text{-}CH_3CO_2)_6$	9.85	2.8	$^5/_2$	20
$Mn^{II}Mn^{III}_2(L)_2(\mu\text{-}CH_3CO_2)_4(ROH)_2$ (L = tridentate ligand, R = H or CH_3)	8.1 (L = saladhp, R = CH_3)	5.3 to 7.1	$^3/_2$	39, 40

[a] The ground state for an $S = {}^5/_2$ Heisenberg spin chain is $S = 0$ or $S = {}^5/_2$ depending on whether it contains an even or odd number of magnetic ions. The ground state of the bulk material is thus a statistical distribution of $S = 0$ and $S = {}^5/_2$ ground states. However, half integer spin chains possess a gapless excitation spectrum. Therefore even at $T = 0$, a band of magnetic states is populated.

six ligands coordinated to each manganese bridges to another manganese.[26–28] These two catagories each have a much narrower range of bond lengths. The mononuclear complexes have Mn–N(imidazole) bonds ranging from 2.18 to 2.28 Å (average = 2.24 for seven different Mn–N bonds), although one of those complexes includes two water molecules and a bidentate croconate ($C_5O_5^-$), which is a poor donor due to its unfavorable bite angle, in its manganese coordination sphere. If the two imidazoles of this complex are not included, the range for the mononuclear complexes is 2.21–2.28 Å with an average of 2.26 Å. The bridged structures have somewhat shorter bond lengths due to the weaker donation of the bridging ligands, with a range of Mn–N(imidazole) bond lengths from 2.15 to 2.23 Å (average = 2.19 Å for 10 different Mn–N bond lengths). Complex **1** fits the mononuclear category and the four different Mn–N(imidazole) bond lengths in its crystal structure range from 2.20 to 2.22 Å, on the low end of the range seen for the other complexes in that category. Complex **3** has three bridging ligands in the coordination sphere of the imidazole-bound manganese and thus fits in the second category. It has a Mn–N(imidazole) bond length of 2.16 Å, on the low end of the distances for the other complexes in that catagory. The polymer **2** has two bridges to other manganese ions, as well as a weakly donating methanol, in each manganese coordination sphere. Its Mn–N(imidazole) bond length of 2.18 Å is close to the average of those in the triply bridged complexes. It is clear that, as expected, the variations in Mn–N(imidazole) bond lengths is mediated by the donor strength of the other ligands in the manganese coordination sphere. Multiple bridges in the coordination sphere, as weaker donors than the corresponding ligands bound to a single metal, result in shorter Mn–N(imidazole) bonds than are observed for mononuclear manganese complexes. This is an important consideration in the manganese coordination spheres in manganese proteins, since many of these proteins are believed to have multinuclear sites with multiple bridging ligands.

Ground State Electronic Structure. The magnetic moment, μ_{eff}, of **1** is 6.01 μ_B at 300 K, compared with the spin-only value of 5.92 μ_B expected for an isolated $S = {}^5/_2$ Mn(II) monomer. The magnetic parameters determined for this complex and those discussed below are listed in Table 7. The electron paramagnetic resonance (EPR) spectrum of a solution of **1** in dmf at 77 K displays a $g = 2$, $m_s = +{}^1/_2 \leftrightarrow -{}^1/_2$ fine structure transition split into six hyperfine lines as expected for a six-coordinate monomeric ^{55}Mn(II) complex. This spectrum is also indicative of the Mn(II) single-ion zero-field splitting parameter being in the $h\nu \gg D$ limit ($h\nu = 0.304$ cm^{-1}).[29] When the solid is diluted in anhydrous $MgSO_4$, the EPR displays a broad derivative-shaped resonance at $g = 2$ with no discernible hyperfine structure.

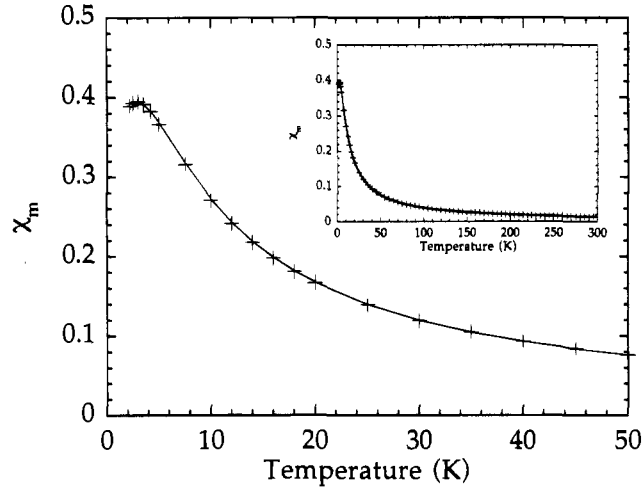

Figure 4. Magnetic susceptibility of **2** collected at 1000 G plotted as χ_M vs temperature from 0 to 50 K, with the fit to the expression in eq 2 for intrachain exchange coupling (solid line). Inset: Same data and fit, from 0 to 300 K. Best fit parameters: $g = 1.95$; $J = -0.25$ cm^{-1}.

Variable-temperature magnetic susceptibility data (2.2–300 K) were collected for **2** in an applied magnetic field of 1000 G. The susceptibility data turn over at ~3 K, indicating the presence of a weak antiferromagnetic exchange interaction. The Hamiltonian appropriate for a linear arrangement of magnetic ions where only nearest-neighbor interactions are important is eq 1.

$$H = \sum_{i=1}^{N} g\beta B S_i - 2J \sum_{i=1}^{N-1} S_i \cdot S_{i+1} \qquad (1)$$

Since there is no low-field resonance in the low temperature EPR spectrum (*vide infra*), the zero-field splitting (D) must be very small and is thus not included in this treatment. For the case of an isotropic intrachain exchange interaction, Heisenberg theory is used. We have successfully fit the variable temperature data of the chain to the Fischer expression[30,31] for an infinite spin chain scaled to $S = {}^5/_2$:

$$\chi_M = (Ng^2\beta^2/3kT)S(S+1)\cdot(1-u)/(1+u) \qquad (2)$$

where $u = T/T_0 - \coth(T_0/T)$, and $T_0 = 2JS(S+1)/k$. The best fit to the data is shown in Figure 4 with spin Hamiltonian parameters $g = 1.95$ and $J = -0.25$ cm^{-1}. There is no evidence of any field-induced long range magnetic order in applied fields up to 5 T. Similarly small exchange couplings (−0.23 to −0.7

(25) Deguenon, D.; Bernardinelli, G.; Tuchagues, J.-P.; Castan, P. *Inorg. Chem.* **1990**, *29*, 3031–3037.
(26) Buchanan, R. M.; Oberhausen, K. J.; Richardson, J. F. *Inorg. Chem.* **1988**, *27*, 971–973.
(27) Buchanan, R. M.; Mashuta, M. S.; Richardson, J. F.; Oberhausen, K. J.; Hendrickson, D. N.; Webb, R. J.; Nanny, M. A. *Inorg. Chem.* **1990**, *29*, 1299–1301.
(28) Rardin, R. L.; A. Bino; Poganiuch, P.; Tolman, W. B.; Liu, S.; Lippard, S. J. *Angew. Chem., Int. Ed. Engl.* **1990**, *29*, 812–814.
(29) Weltner, W. *Magnetic Atoms and Molecules*; Dover Publications, Inc.: New York, 1989.
(30) Dingle, R.; Lines, M. E.; Holt, S. L. *Phys. Rev.* **1969**, *187*, 643.
(31) Fischer, M. E. *Am. J. Phys.* **1964**, *32*, 343.

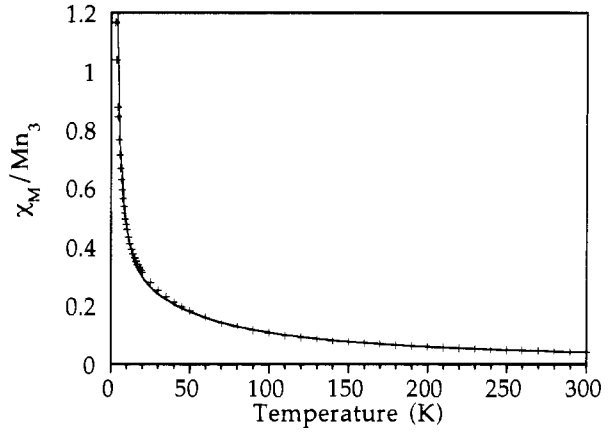

Figure 5. Magnetic susceptibility of **3** collected at 10 000 G plotted as χ_M vs temperature, with the fit to eq 4 (solid line) with g fixed at 2.00 and $J = -1.7$ cm^{-1}.

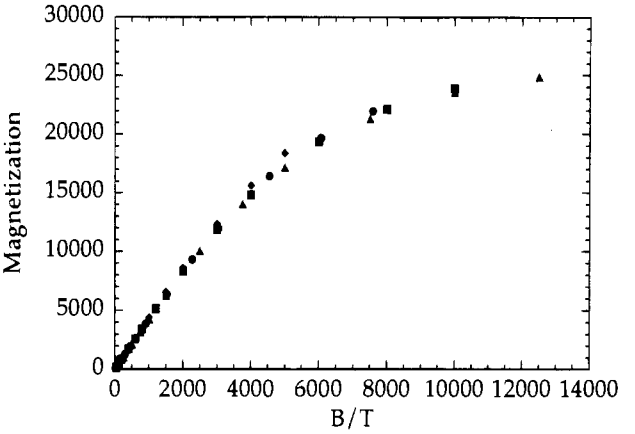

Figure 6. Magnetization data for **3** plotted as a function of B/T. Data were collected at 2.0 K (▲), 2.5 K (■), 3.3 K (●), and 5.0 K (◆).

cm^{-1}) have been observed previously in a series of Mn(III) chains with carboxylate bridging in an anti−anti manner.[32]

The EPR spectrum of a dmf solution of **2** produces an almost identical spectrum to that of **1**, indicating that **2** dissociates into monomeric Mn(II) units in solution. This is confirmed by determination of the molecular weight in a dmf solution by vapor pressure osmometry, which gives a molecular weight of 400, consistent with the formula weight of one link of the chain in **2**. The EPR spectra of the solid **2** diluted in anhydrous $MgSO_4$ at both 77 and 5.5 K show only a broad derivative shaped signal centered at $g = 2$, with no discernible hyperfine splitting and no apparent low field features.

Variable-temperature magnetic susceptibility data (2.8−300 K) were also collected for **3**. The Hamiltonian (3), appropriate for an exhange-coupled trinuclear cluster was employed in the

$$H = g\beta B\cdot(S_1 + S_2 + S_3) - 2J(S_1\cdot S_2 + S_2\cdot S_3) \qquad (3)$$

analysis of the magnetic data for **3**, where S_1 and S_3 are the spins of the terminal Mn(II) ions and S_2 is the spin of the central Mn(II) ion. (Note that these do not correspond to the crystallographic numbering scheme.) This model assumes that the coupling between the terminal Mn(II) ions ($J_{1,3}$) is zero. The data were fit as the molar magnetic susceptibility per trinuclear cluster to eq 4, which is derived from the field-independent Van

$$\chi_M = (Ng^2\beta^2/3kT)\frac{[\sum_i S_i(S_i+1)(2S_i+1)\exp(-E_i/kT)]}{[\sum_i (2S_i+1)\exp(-E_i/kT)]} \qquad (4)$$

Vleck equation. The energies, E_i, of the states that comprise the spin ladder of the trimer are given by eq 5, where, according

$$E_i = -J[S_T(S_T+1) - S_{13}(S_{13}+1) - {}^{35}/_4] \qquad (5)$$

to the standard vector coupling rules, S_{13} and S_T possess allowed values $S_1 + S_3 \ldots |S_1 - S_3|$, and $S_{13} + S_2 \ldots |S_{13} - S_2|$, respectively.[33] The best fit to the χ_M vs T data with g fixed at 2.00 is obtained with $J = -1.7$ cm^{-1} and is shown as the solid line in Figure 5. When both g and J are allowed to vary, a slightly improved fit is obtained with the parameters $g = 1.96$ and $J = -1.4$ cm^{-1}. The ground state is therefore $|{}^5/_2, 5\rangle$ ($|S_T, S_{13}\rangle$ basis) and is energetically separated from the $|{}^3/_2, 4\rangle$ and $|{}^7/_2, 5\rangle$ lowest excited states by $5J$ and $7J$ respectively.

Variable-temperature, variable-field magnetization data (2−5 K in applied fields up to 2.5 T) were collected for **3** in order to determine the zero-field splitting of the sextet ground state ($|{}^5/_2, 5\rangle$), to assess the validity of the $J \gg D$ model used in the analysis of the susceptibility data, and to determine the individual axial single ion zero-field splitting parameters D_i ($i = 1-3$). Isothermal magnetization data are plotted as a function of B/T in Figure 6. Data acquired at different temperatures are superimposable and show no evidence of nesting behavior at applied fields as high as 2.5 T. This is indicative of small zero-field splittings of the sextet ground state, no appreciable population of higher $|S_T, S_{13}\rangle$ spin states at the temperatures studied, and negligible field induced mixing between the thermally populated spin states.

The Hamiltonian (6) was used to operate upon the ground state sextet ($|S_T = 5/2, m_s\rangle$) basis functions. In order to avoid

$$H = g_{\parallel}\beta B\cdot S_z + g_{\perp}\beta B\cdot(S_x + S_y) + D[S_z^2 - {}^1/_3 S(S+1)] \qquad (6)$$

problems with overparameterization, $g_{\parallel}$ was held constant at 2.00 while $g_{\perp}$ and D were allowed to vary. Diagonalization of the resultant 6 × 6 matrix resulted in six energy eigenvalues which were subsequently substituted into the thermodynamic expression for the magnetization (7) where $M_{\cos\theta}$ describes the molar

$$M_{\cos\theta} = -N\frac{[\sum_i \partial E_i/\partial B \exp(-E_i/kT)]}{[\sum_i \exp(-E_i/kT)]} \qquad (7)$$

magnetization per trimer with the magnetic field direction at an angle θ with respect to the principle axis of the trimer. The partial derivatives of the eigenvalues with respect to the applied magnetic field, $\partial E_i/\partial B$, were calculated exactly using the Hellman−Feynman theorem.[34] A numerical integration technique making use of the Labatto quadrature[35] was used in the determination of the powder averaged molar magnetization:[36]

$$M_{av} = {}^1/_2\int_0^{\pi} M_{\cos\theta}\sin\theta\, d\theta \qquad (8)$$

The best fit of the expression to the data yielded $g_{\perp} = 1.99$ and $D = -0.38$ cm^{-1}. Using tensor operator methods and the recursion relations found in refs 37 and 38, the zero-field

(32) Kirk, M. L.; Lah, M. S.; Raptopoulou, C.; Kessissoglou, D. P.; Hatfield, W. E.; Pecoraro, V. L. *Inorg. Chem.* **1991**, *30*, 3900−3907.
(33) Kambe, K. J. *Phys. Soc. Jpn.* **1950**, *5*, 48.
(34) Vermas, A.; Groeneveld, W. L. *Chem. Phys. Lett.* **1974**, *27*, 583−585.
(35) Scarborough, J. P. *Numerical Mathematical Analysis*; Oxford University Press: New York, 1971.
(36) Marathe, V. R.; Mitra, S. *Chem. Phys. Lett.* **1974**, *27*, 103−106.
(37) Bencini, A.; Gatteschi, D. *EPR of Exchange Coupled Systems*; Springer-Verlag: Berlin, 1990.

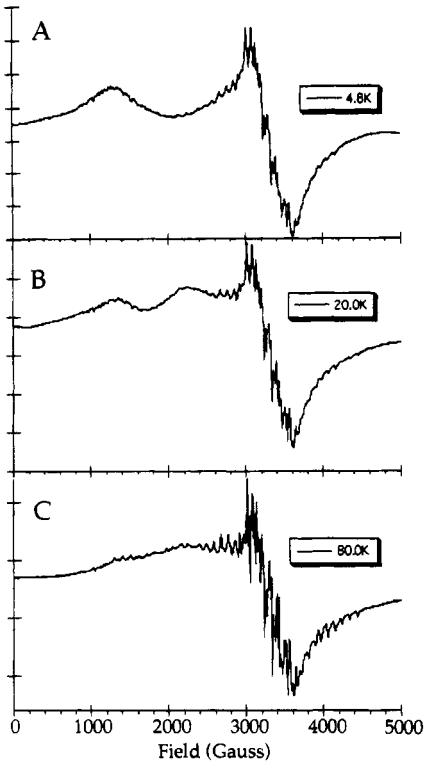

Figure 7. X-band EPR spectra of microcrystalline **3** dispersed in anhydrous $Mg(SO_4)$ at 10 mW and various temperatures: (A) 4.8 K; (B) 20 K; (C) 80 K.

splitting of the $|^5/_2, 5\rangle$ ground state can be related to that of the three single ions that comprise the trimer:

$$D = 0.615\,(D_1 + D_3) + 0.357D_2 \qquad (9)$$

If it is assumed that the single ion zero-field splitting parameters for the central and terminal Mn(II) ions are equivalent then the individual $D_i = -0.24\ cm^{-1}$.

A solid state powder EPR of **3** dispersed in anhydrous $MgSO_4$ was used to determine independently the magnitude of the ground-state zero field splitting parameter D. These spectra are quite rich and vary significantly with temperature. Figure 7 compares the spectra at 4.8, 20.0, and 80.0 K. In each of these spectra, the $g = 2$ region consists of somewhat different but equally complicated multiline (>20-line) features. The 4.8 K spectrum contains an additional strong positive component centered around $g = 5.1$. As the temperature increases, the $g = 5.1$ feature decreases in intensity, disappearing by the time the temperature reaches 40 K. A new broad positive feature grows in at $g = 2.9$ which maximizes around 20 K, and disappears between 40 and 80 K. Using the exchange coupling value of $J = -1.7\ cm^{-1}$ obtained from the variable temperature magnetic susceptibility data, the population of the $|^5/_2, 5\rangle$ ground state at 4.8 K is >90%. In this case the $g = 5.1$ resonance can be assigned as the $m_s = +^1/_2 \leftrightarrow -^1/_2$ fine structure transition in the perpendicular direction.[29] Fitting the perpendicular direction energy eigenvalue differences to match the resonance condition ($h\nu = 0.304\ cm^{-1}$) yields the zero-field splitting parameter directly. The value obtained for $|D|$ in this manner is $0.19\ cm^{-1}$, in good agreement with the variable-temperature, variable-field magnetization results. In an analogous manner to the variable-temperature, variable-field magnetization studies, the zero-field splitting of the $|^5/_2, 5\rangle$ ground state can be related to that of the three single ions that comprise the trimer yielding individual $|D_i| = 0.12\ cm^{-1}$. Note that the sign of the zero-field splitting was not determined by this EPR study.

The EPR spectrum of a methanol/ethanol solution of **3** is dominated by the same six-line spectrum as solutions of **1** and **2**, with an additional weak feature around $g = 5$. The EPR spectrum of a dmf/toluene solution of **3** displays the $g = 2$ six-line signal as its dominant feature; however it also has weak features devoid of any hyperfine splitting at $g = 2.70$ (positive), $g = 6.1$ (positive), and $g = 1.67$ (negative). Additionally, a positive feature is observed at $g = 2.27$ with at least eight hyperfine lines separated by 44 G. This hyperfine splitting is typical of dimeric Mn(II) species. Therefore, **3** may dissociate into monomeric Mn(II) units in dmf as observed for **2**, but with some equilibrium concentration of an additional multinuclear species. This kind of solvent dependence on the appearance of the EPR spectrum has also been observed for $Mn^{II}Mn^{III}_2(saladhp)_2(\mu\text{-}CH_3CO_2)_4(CH_3OH)_2$.[39]

The magnetic parameters for **3** may be compared to previously reported values for the bis(μ-carboxylato-*O*,*O*′)(μ-carboxylato-*O*)-bridged Mn(II) trimers $Mn_3(CH_3CO_2)_4(bpy)_2$ ($J = -2.2\ cm^{-1}$ for the Hamiltonian in eq 3 and fit to the same parameters as **3**)[21] and $Mn_3(CH_3CO_2)_6(BIPhMe)_2$ ($J = -2.8\ cm^{-1}$ by varying J_{13} and θ rather than g).[20] As for both of these complexes, μ_{eff} for **3** at room temperature is around 10.0 μ_B which is somewhat lower than the value expected for 3 uncoupled $S = ^5/_2$ ions with $g = 2$ (10.25 μ_B). This comparison is summarized in Table 7. Considering the differences in which parameters were varied to produce the fits in these three studies of Mn(II) trimers, it is not clear that the differences obtained in the values of J are significant. It may be somewhat surprising that the single-atom phenolate bridge in **3** does not mediate stronger exchange coupling than the all-carboxylate bridging structures of the other two trinuclear complexes.

Another variation on the linear trinuclear manganese complex to which this may be compared is the complex $Mn^{II}Mn^{III}_2(saladhp)_2(\mu\text{-}CH_3CO_2)_4(CH_3OH)_2$.[39] This complex also contains a meridional tridentate ligand and two bridging acetates between each pair of Mn ions, which are 3.55 Å apart. However, the terminal manganese ions are in the Mn(III) oxidation state and the ligating groups of saladhp are phenolate, imine, and alkoxide, with the alkoxide bridging the manganese. This provides a (μ-alkoxo)bis(μ-carboxylato-*O*,*O*′) bridging set, similar to the geometry which would occur upon a "carboxylate shift" of the (μ-carboxylato-*O*) bridge in **3** to a (μ-carboxylato-*O*,*O*′) bridge coupled with manganese oxidation.[17] The exchange coupling between the manganese in this complex is $J = -7.1\ cm^{-1}$. A series of similar $Mn^{II}Mn^{III}_2L_2(\mu\text{-}CH_3CO_2)_4(ROH)_2$ complexes, where L is a tridentate ligand and R is H or CH_3, have a range of exchange coupling constants $-5.3\ cm^{-1} > J > -7.1\ cm^{-1}$.[40] These are somewhat larger than the values of the Mn^{II}_3 complexes, which is generally observed for higher manganese oxidation states; however, the coupling remains rather weak. It does not appear, therefore, that the "carboxylate shift" between the monatomic and triatomic bridging modes has a large effect on the magnetic coupling in these systems.

Summary

The crystallographically defined complexes **1**–**3** show three very different structural motifs provided by the imidazole-containing tridentate ligand 5-NO_2-salimH$^-$. These structural

(38) Scaringe, R. P.; Hodgson, D. J.; Hatfield, W. E. *Mol. Phys.* **1978**, *35*, 701–713.

(39) Li, X.; Kessissoglou, D. P.; Kirk, M. L.; Bender, C. J.; Pecoraro, V. L. *Inorg. Chem.* **1988**, *27*, 1–3.

(40) Kessissoglou, D. P.; Kirk, M. L.; Lah, M. S.; Li, X.; Raptopoulou, C.; Hatfield, W. E.; Pecoraro, V. L. *Inorg. Chem.* **1992**, *31*, 5424–5432.

differences are produced by small changes in carboxylate stoichiometry or type, showing that this ligand is capable of producing a rich variety of manganese complexes containing the biologically important imidazole and carboxylate ligands. The manganese(II)−imidazole bond lengths of these complexes have been considered along with other 6-coordinate manganese(II)−imidazole complexes to provide a range of "normal" manganese(II)−imidazole bond lengths for comparison to the lengths of similar bonds in biological systems. The range of bond lengths in the model systems demonstrates that the Mn−N distances in multiply bridged systems should be expected to be somewhat shorter than those in mononuclear systems due to the weaker donor strength of the other ligands which interact with more than one Mn ion.

The magnetic studies presented here show that the anti−anti formate bridging configuration provides only very weak exchange coupling ($J = -0.25$ cm^{-1}) between the manganese(II) ions in the polymer, **2**. The coupling in **3** ($J = -1.7$ cm^{-1}) is nearly an order of magnitude larger than in **2**, but approximately the same as in the bis(μ-carboxylato-*O*,*O*')(μ-carboxylato-*O*)-bridged Mn^{II}_3 complexes, despite the replacement of one of the triatomic carboxylate bridges by the monatomic phenolate bridge. The previously reported complexes $Mn^{II}Mn^{III}_2L_2(\mu\text{-}CH_3CO_2)_4(ROH)_2$, which correspond to a "carboxylate shift" of the monatomically bridging carboxylate in **3** to a triatomic bridge, show a somewhat stronger exchange coupling. The coupling is still quite weak, however, considering the higher valent manganese, which appears to indicate that the "carboxylate shift" of one bridging acetate does not by itself impose a significant change in the exchange interaction.

Acknowledgment. Funding for this work was provided by an NIH grant (GM39406) and an NIH postdoctoral fellowship to M.J.B. (GM15102).

Supporting Information Available: Full experimental details and structural parameters for **1** and **2** (Table S1), fractional coordinates for all non-hydrogen atoms in **1** (Table S2) and **2** (Table S7), fractional coordinates for hydrogen atoms in **1** (Table S3) and **2** (Table S8), anisotropic thermal parameters for non-hydrogen atoms in **1** (Table S4) and **2** (Table S9), bond lengths for **1** (Table S5) and **2** (Table S10), bond angles for **1** (Table S6) and **2** (Table S11), ORTEP diagrams for each independent molecule in the asymmetric unit of **1** with complete numbering systems (Figures S1 and S2), the ORTEP diagram of **2** with the complete numbering system (Figure S3), and a representative portion of the unit cell of **2** (Figure S4) (21 pages). Ordering information may be found on any current masthead page. The structure of **3** has been previously reported[17] and deposited in the Cambridge crystallographic data base.

IC9406704